JMEPEG (2014) 23:2591–2598
DOI: 10.1007/s11665-014-0906-y

1059-9495/$19.00

Simulations of Mechanical Response of Superelastic NiTi Helical Spring and its Relation to Fatigue Resistance

P. Sedlák, M. Frost, A. Kruisová, K. Hiřmanová, L. Heller, and P. Šittner

(Submitted October 10, 2013; in revised form January 17, 2014; published online February 20, 2014)

Behavior of NiTi shape memory alloys under complex loading is still a subject of both experimental and theoretical investigations. One of the simplest geometries, in which the material is loaded in combined mode and which has also several practical applications, is a simple helical spring. In this contribution, mechanical response of NiTi superelastic spring is analyzed in detail by numerical simulation and the results are compared to experiments. The simulations show complex stress state, which develops during spring stretching. Analyzing fatigue tests with respect to simulated behavior allowed us to find relation between fatigue resistance and periodic changes in volume fraction of martensite induced by cyclic mechanical loading. The work also underlines an extension of the range of stroke amplitudes guaranteeing enhanced life performance of the spring when material transforms through the R-phase.

Keywords helical spring, non-proportional loading, numerical modeling, R-phase, shape memory alloys

1. Introduction

Shape memory alloys (SMA) are metallic materials exhibiting unusual properties of being able to sustain and recover large strains and to "remember" the initial configuration and return to it with temperature change. These properties arise from a rearrangement of the crystal lattice associated with the so-called martensitic phase transformation, which can be induced by variation of temperature and/or variation of the applied mechanical load. Moreover, specific types of internal structure of the martensitic phase can develop depending on the loading conditions. These phenomena give rise to a very complex thermomechanical behavior, which classifies SMA into the group of so-called smart materials and makes them attractive for utilization in applications (Ref 1-3).

Although the basic deformation characteristics of SMA in simple loading modes have been extensively investigated in past decades, noticeably less attention has been paid to response during a general (non-proportional) thermomechanical loading. This gap was aimed to be filled in within so-called "Roundrobin SMA modeling" activity (Ref 4), in which an extensive set of experimental data on general loading of NiTi wire combining tension, torsion, and temperature was gained and made available to wide research community. Figure 1 presents an illustrative example. In the upper part of all three graphs, dependence of torque on angular displacement for a single sample loaded in torsion is shown in blue. At first glance, the plots resemble a typical transition from a superelastic response (material recovers its initial shape by unloading) to a pseudoplastic response with remanent strain as the temperature decreases. However, all the measurements were performed at the same temperature (40 °C) and it is actually the value of prestress in tension (200, 300, and 380 MPa, respectively) which was varied and led to an essential change of response to cyclic twisting due to the effect of combined axial and shear stress. A significant change of response is also observed in dependence of axial strain on angular displacement presented in the same Figure in green. Surprisingly enough, such a peculiar evolution of response can arise during this type of cyclic loading even at a (specific) constant external prestress (see Ref 4). These results demonstrate how sensitive the material response can be to changes in loading conditions when multiple deformation mechanisms come into play.

Recently, several "macro-"models focused on mechanical response of SMA to general thermomechanical loading, e.g., (Ref 5-11). They were developed within the continuum mechanics and include processes which occur in the material at microscopic level (phase transformations and martensite domains reorientation) and have an impact at macroscopic level (inelastic strain) by introduction of internal variables. These variables extend description of thermodynamic state in a material point and, as like as external variables (stress, strain, and temperature), they appear in thermodynamic potential (energy function). Most importantly, they allow capturing dissipation connected to the internal processes. Based on exploitation of the dataset (Ref 4), a novel thermomechanical three-dimensional model of NiTi-based SMA was developed and implemented into a finite element package in Ref 12. It features a novel form of dissipation function combining transformation and reorientation contributions and includes R-phase transition and material anisotropy.

This article is an invited paper selected from presentations at the International Conference on Shape Memory and Superelastic Technologies 2013, held May 20-24, 2013, in Prague, Czech Republic, and has been expanded from the original presentation.

P. Sedlák, Institute of Thermomechanics ASCR, Prague, Czech Republic; and Faculty of Nuclear Sciences and Physical Engineering, Czech Technical University in Prague, Prague, Czech Republic; **M. Frost**, Institute of Thermomechanics ASCR, Prague, Czech Republic; and New Technologies - Research Center, University of West Bohemia, Plzenu, Czech Republic; **A. Kruisová**, Institute of Thermomechanics ASCR, Prague, Czech Republic; and **K. Hiřmanová , L. Heller,** and **P. Šittner**, Department of Functional Materials, Institute of Physics ASCR, Prague, Czech Republic. Contact e-mail: psedlak@it.cas.cz.

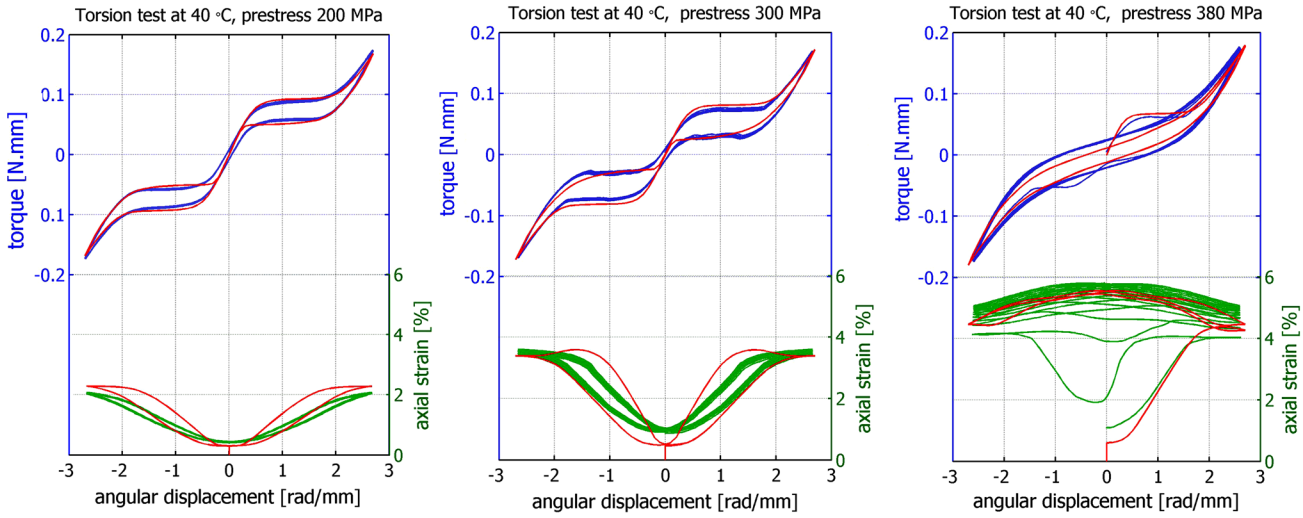

Fig. 1 Combined tension-torsion tests at various axial preloads and a constant temperature 40 °C (blue and green lines—experiment, red lines—simulations) (Color figure online)

In this study, the novel model is employed to better understand evolution of stress state and phase composition of a helical NiTi spring subject to stretching. The SMA spring is an example of a product, which has a very simple geometry, and, at the same time, even a simple stretching induces a complex stress state in it. For its relatively broad application potential (Ref 13), several approaches of SMA spring simulation were already published in literature. A relatively accurate agreement for low stroke amplitudes was achieved by simplified models employing one-dimensional constitutive modeling of SMA (e.g., (Ref 14)). Large deformation of SMA spring leads to significant change of the curvature of spring coils, and an accurate stress analysis requires three-dimensional finite element simulation with constitutive models of SMA describing response to general loading (Ref 15, 16).

The presented numerical analysis confirms good performance of the novel SMA model (Ref 12) and reveals that complex stress states and phase distribution emerge and evolve during stretching. Within broader research focused on fatigue properties and failure of braided stents (Ref 17), a systematic experimental investigation of mechanical response of such a spring was also conducted. Although simulations did not involve any specific fatigue mechanism, comparison of results of the numerical analysis with the experimental data indicates an intriguing relation between periodic changes in volume fraction of martensite in the NiTi spring induced by cyclic mechanical loading and its fatigue performance. The transformation of material through intermediate R-phase was also analyzed, and simulated results show that R-phase has considerable influence on overall mechanical response and fatigue resistance.

2. Model Description

During complex quasi-static loading, the total mechanical response of SMA is determined by interplay of non-dissipative (elasticity) and dissipative processes (phase transformations and reorientation). Rate-independent nature of these dissipative processes in isothermal setting is generally accepted (Ref 18), and it was experimentally confirmed even for complex loading paths and complex specimen geometries (Ref 19). As discussed above, their mutual interaction makes the response quite intricate requiring an advanced model for comprehensive macroscopic description. An alternative way to common definition of particular domain(s) of admissible forces (given by yield function) together with a flow rule may be utilization of the framework of so-called generalized standard materials (models) described e.g., in Ref 20. The model is assembled by definition of a particular form of energy function (thermodynamic potential) and dissipation function.* The constitutive response is then given by so-called principle of minimum dissipation potential, i.e., by minimization of sum of dissipation function and time derivative of energy function with respect to thermodynamic fluxes (Ref 21). Of course, apt choice of the functions requires "a good knowledge of both reversible and irreversible mechanisms operating within the considered material" (Ref 20) and it is vital for construction of physically meaningful model.

Exploitation of set of experiments focused on non-proportional loading of NiTi wires in Ref 4 leads to formulation of a novel constitutive model described in Ref 12, 22. In addition to total strain, ε, and temperature, T, two scalar internal variables—volume fraction of martensite, ξ, and volume fraction of R-phase, η—and one tensorial internal variable—traceless inelastic strain related to transformation, ε^{in}—are introduced. The Helmholtz free energy and dissipation functions take the following forms (see Ref 12 for more details):

$$f(T,\epsilon,\epsilon^{\mathrm{in}},\xi)=\frac{1}{2}K(\xi,\eta)\,tr(\epsilon)^2 + G(\xi,\eta)\left\|\mathrm{dev}(\epsilon)-\epsilon^{\mathrm{in}}\right\|^2+\Delta s^{\mathrm{AM}}(T-T_0)\xi + \Delta s^{\mathrm{AR}}\left(T-R_{\mathrm{s}}-\frac{\eta}{1-\xi}\frac{R_{\mathrm{f}}-R_{\mathrm{s}}}{2}\right)\eta+Q(T)$$

where $Q(T)$ is a term depending on temperature only, hence not relevant under isothermal conditions studied here, and

*Let us note that there is a direct relation between dissipation function and corresponding yield function through Legendre transformation if some mathematical assumptions are satisfied.

$$d(T,\epsilon^{\text{in}},\xi,\dot{\epsilon}^{\text{in}},\dot{\xi}) = \begin{cases} \Delta s^{\text{AM}}[T_0 - M_s + \xi(M_s - M_f)]\,\dot{\xi} + \sigma^{\text{reo}}(T)\left\|\dot{\epsilon}^{\text{in}}\right\|, & \text{if } \dot{\xi} \geq 0, \\ \Delta s^{\text{AM}}[T_0 - A_f + \xi(A_f - A_s)]\,\dot{\xi} + \sigma^{\text{reo}}(T)\left[\left\|\frac{\dot{\xi}}{\xi}\epsilon^{\text{in}}\right\| + \left\|\dot{\epsilon}^{\text{in}} - \frac{\dot{\xi}}{\xi}\epsilon^{\text{in}}\right\|\right], & \text{if } \dot{\xi} < 0. \end{cases} \quad \text{(Eq 2)}$$

Brief description of material parameters can be found in Tab. 1. As a simple approximation,** elastic isotropy of all phases is assumed and the Reuss model of elastic properties is used in the present formulation, i.e., bulk and shear moduli of multiphase material are computed from values of constituent phases employing the inverse rule of mixtures. Instead of bulk moduli, corresponding values of more common Young modulus are presented in the table; they fit well with experimental measurements published in Ref 24.

Constraints on internal variables, given by natural restrictions on a volume fraction and by existence of maximum strain due to transformation to martensite, can be condensed to the indicator function:

$$I(\epsilon^{\text{in}},\xi,\eta) = \begin{cases} 0, & \text{if } 0 \leq \xi \leq 1,\ 0 \leq \eta \leq 1-\xi,\ \langle\epsilon^{\text{in}}\rangle \leq \xi, \\ +\infty, & \text{else.} \end{cases} \quad \text{(Eq 3)}$$

The specific form of function denoted by angle bracket capturing both transformation strain anisotropy and tension-compression asymmetry was taken as:

$$\langle\epsilon^{\text{in}}\rangle = \frac{I_2(D\epsilon^{\text{in}})}{k}\frac{\cos\left(\frac{1}{3}\arccos\left(1 - a\left(I_3(D\epsilon^{\text{in}}) + 1\right)\right)\right)}{\cos\left(\frac{1}{3}\arccos(1-2a)\right)}, \quad \text{(Eq 4)}$$

where

$$I_2(x) = \sqrt{\frac{2}{3}x_{ij}x_{ij}} \quad \text{and} \quad I_3(x) = 4\frac{\det(x)}{(I_2(x))^3}, \quad \text{(Eq 5)}$$

k is a material parameter representing the maximum transformation strain in tension, a characterizes the tension-compression asymmetry and linear mapping $\mathbf{D}$: $R^6 \rightarrow R^6$ defined by material parameters A, B, φ, L, M, N describes transformation strain anisotropy (Ref 12).

As pointed up in Ref 21, combination of principle of minimum potential energy and principle of minimum dissipation potential may be advantageously used in numerical implementation of the constitutive model to find the overall mechanical response of an SMA body in quasistatic loading. After time discretization, the problem may be split into two complementary subproblems, which are to be solved consecutively. The first one determines displacement and can be solved by common finite element software packages; the second one leads to solving a reduced time-incremental minimization problem in each material point at a time step t in the form:

$$\text{Minimize } f(T_t,\epsilon_t,\epsilon^{\text{in}},\xi,\eta) + d(T_t,\epsilon_{t-1},\xi_{t-1},\epsilon^{\text{in}} - \epsilon^{\text{in}}_{t-1},\xi - \xi_{t-1}) + r(\epsilon^{\text{in}},\xi,\eta) \text{ subject to } (\epsilon^{\text{in}},\xi,\eta). \quad \text{(Eq 6)}$$

Function r denotes the regularization of the indicator function I as chosen in Ref 12. The minimization problem is solved within UMAT subroutine, which allows to implement user-defined constitutive models into Abaqus finite element software package. For more details on numerical treatment of the model see Ref 12, 22. As an illustration of model performance, experiments presented in Fig. 1 were simulated (for more detailed validation see Ref 12). The numerical results (red lines) were added to Fig. 1 for comparison.

Let's summarize the main highlights of introduced model relevant for present study. The model takes into account:

- Joint influence of stress and temperature on any of included phase transition.
- Both dissipations related to transformation to martensite and dissipation related to martensite reorientation; the latter dissipation can occur even when there is no change in volume fraction of martensite.
- Difference of Young and shear moduli of all included phases (Austenite, R-phase, and martensite).
- Tension-compression asymmetry observed e.g., in Ref 25-27.
- Anisotropy of transformation strain due to strong texture, see e.g., (Ref 28).

3. Simulation of NiTi Helical Spring

The simulation of loading of NiTi helical spring was performed in the finite element software Abaqus. The simulated geometry approximated shape of experimentally examined samples (Fig. 2) and was generated as an ideal helix with 2.6 coils, the initial outer diameter being 3.2 mm, the initial length 3.9 mm, and the wire diameter 200 μm. The geometry was meshed by 9984 (32 through wire cross section) eight-node linear hexahedral elements with reduced integration (C3D8R). It was tested that additional refinement of the mesh (48 elements through the wire cross section) led to numerical results differing only less than 1% from the coarser mesh. Material parameters of the wire are summarized in Table 1. They correspond to the parameters used in Ref 12 for simulations of combined loading of the Fort Wayne Metals (FWM) NiTi#1 superelastic 200 μm wire. The same wire with the identical radius and heat treatment was also used for fabrication of experimental samples (see section 4).

**Anisotropy of elastic properties was experimentally confirmed in Ref 23. However, because of difficulties with complete determination of stiffness tensor (5 independent constants for transverse isotropic material), assumption of elastic isotropy was adopted (similarly to Ref 5-10) and elastic properties were determined only by two constants—Young modulus E and shear modulus G. This simplification can only slightly influence the simulation as only shear and tensile/compressive stress components are significant in loaded spring.

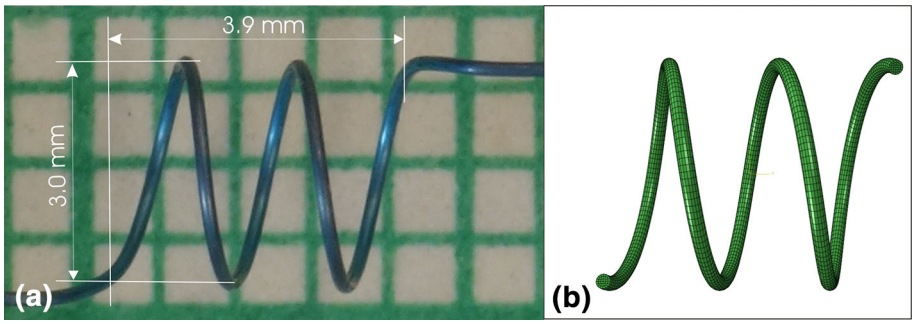

Fig. 2 (a) Superelastic NiTi helical spring—examined sample and (b) Image of simulated geometry and finite element mesh

Table 1 Material parameters used in all numerical simulations in this study together with their brief description

Parameter	Value	Unit	Brief description
E^{A}	71	GPa	Young modulus of austenite
E^{M}	41	GPa	Young modulus of martensite
E^{R}	41	GPa	Young modulus of R-phase
G^{A}	25	GPa	Shear modulus of austenite
G^{M}	23	GPa	Shear modulus of martensite
G^{R}	14	GPa	Shear modulus of R-phase
T_0	−20	°C	Equilibrium temperature of A and M phases
M_s	−22	°C	Martensite start temperature
M_f	−24	°C	Martensite finish temperature
A_s	−17	°C	Austenite start temperature
A_f	−13	°C	Austenite finish temperature
σ_0^{reo}	160	MPa	Reorientation stress at T_0
Σ^{reo}	0.9	MPa/°C	Change of reorientation stress with temperature [see (Ref 12)]
Δs^{AM}	0.364	MPa/°C	Difference between entropy of A and M
Δs^{AR}	0.121	MPa/°C	Difference between entropy of A and R
R_s	39	°C	Initial A to R transformation temperature
R_f	1	°C	Final A to R transformation temperature
k	0.07	···	Maximum transformation strain in tension
a	0.9	···	Tension-compression asymmetry parameter
A, B, ϕ	1, 1, 0	···	Parameters of transformation anisotropy
L, M, N	1, 1.44, 1.44	···	Parameters of transformation anisotropy
c^{reg}	0.01	MPa	Material parameter (see Ref 12)
E^{int}	30	MPa	Material parameter (see Ref 12)

The bulk modulus K used in Eq. 1 can be recalculated from E and G by standard formula

The material parameters were derived from tension-torsion experiments (Ref 4) and include description of anisotropy of transformation strain surface, i.e., feature related to strong wire [111] texture, which considerably affects wire response in complex loading. The only parameter, which was not directly obtained from experiments on this wire—the ratio of transformation strain in tension versus transformation strain in compression—was set to 3/2, which is a typical value obtained in experiments on drawn NiTi wires or tubes in direction of drawing (Ref 29). The symmetry axis of transverse isotropy of the material was supposed to follow the axis of the wire forming the spring.

The loading and unloading of the spring were simulated by gradual change of prescribed displacement in the direction of the spring axis at one end of the spring while holding the second spring end. In order to restrict untwisting of the spring, the center of the boundary cross sections was kept on the plane defined by initial position of this point and the spring axis. The maximum stroke was 19.5 mm. In one case, rotation around the axis, which is perpendicular to the spring axis and goes through the cross sections' center, was allowed. In the other case, this rotation was not allowed. The former constraint leads to almost identical results as periodic boundary condition with translation simulating an infinite spring. The difference in obtained results with different boundary conditions was app. 5% up to stroke of 12 mm. As the simulation with allowed rotation approximated better experimental observations in a broader range of strokes, we employed these boundary conditions in what follows.

Figure 3 shows simulated force-stroke response at temperature 37 °C together with contour plots from the center of the spring. The latter provide basic information about evolution of simulated volume fraction of martensite and distribution of two significant components of stress tensor: tensile/compressive stress parallel to the wire axis and shear stress acting on wire cross section in angular direction.

The austenite-R-phase transformation dominates to the first part of the force-stroke curve (approx. to the stroke of 6 mm).The R-phase induced mainly by shear considerably lowers the effective modulus of the spring as it is a soft phase in

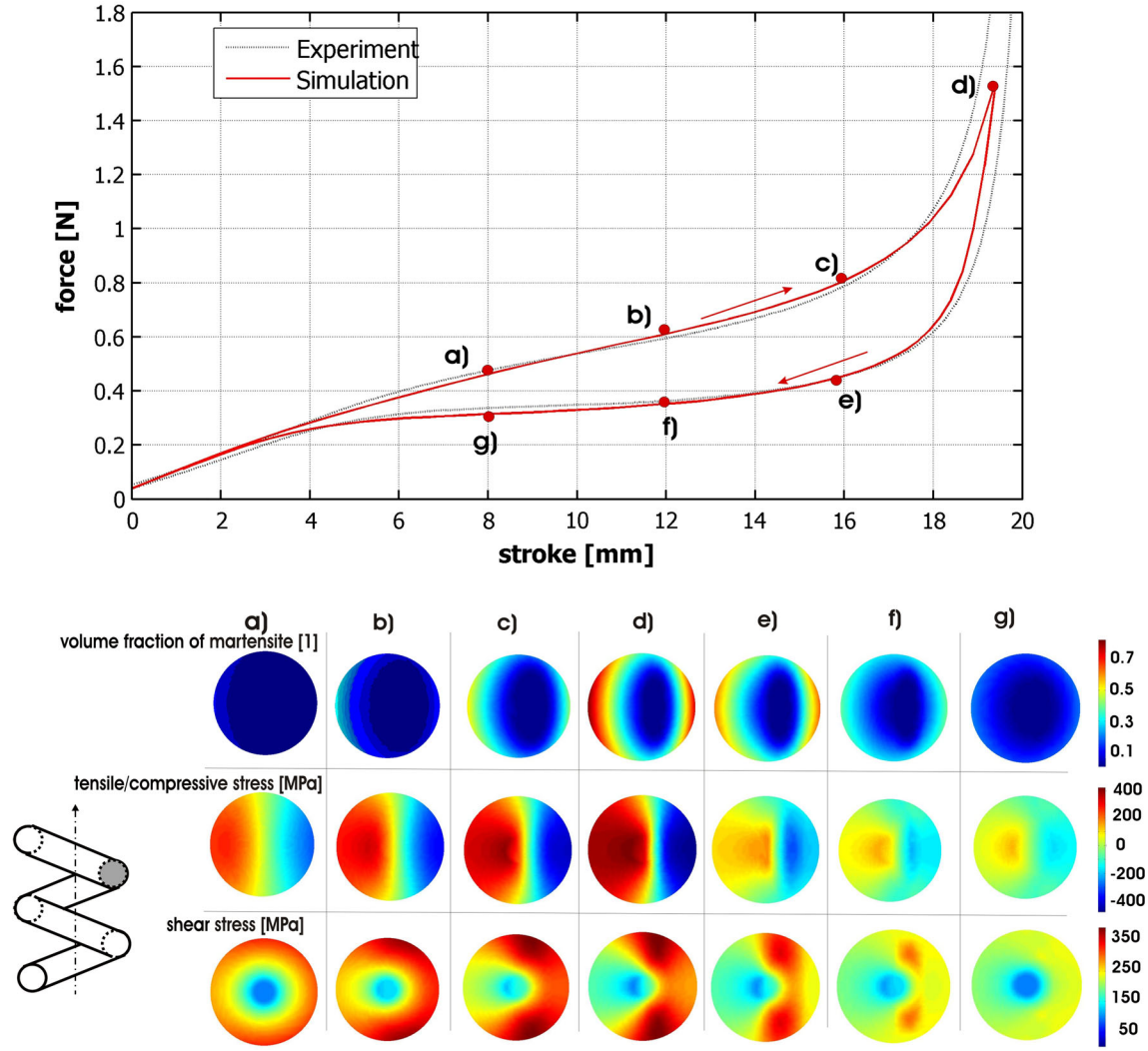

Fig. 3 Simulated and experimental force-stroke dependence of superelastic NiTi helical spring at 37 °C. Contour plots below show computed distributions of volume fraction of martensite, tensile/compressive stress, and shear stress throughout wire cross section in the central part of the spring

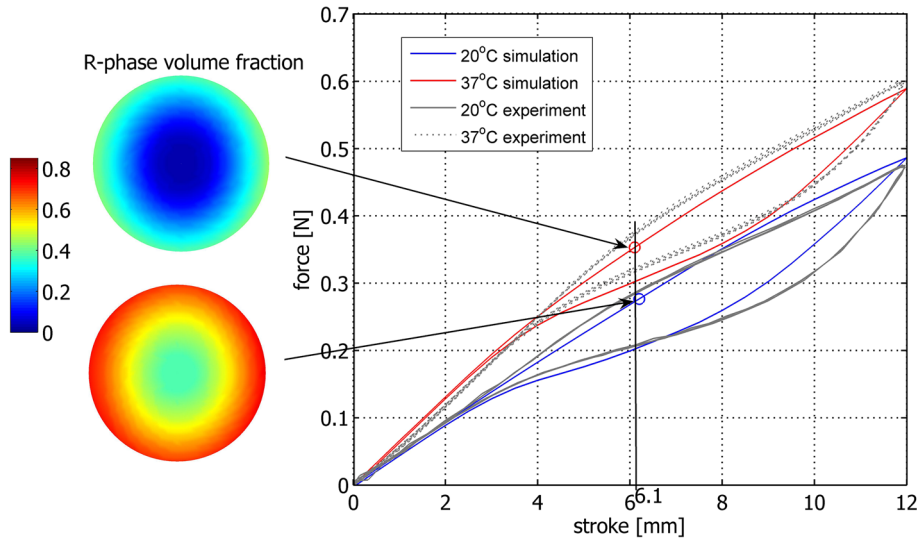

Fig. 4 Simulated and experimental force-stroke dependence for two different temperatures (20 and 37 °C) together with simulated distribution of R-phase volume fraction at the points (depicted by circles) of initiation of martensitic transformation

comparison with austenite (see Table 1). The spring response in this part is very sensitive to changes in temperature, which is given by the steep Clausius-Clapeyron slope for R-phase (Ref 30). Distribution of the volume fraction of R-phase is presented in Fig. 4, where a subloop response of the spring up to stroke of 12 mm is depicted and also the simulation of the behavior at 20 °C was added to show strong temperature dependence.

Figure 4 also shows the first occurrence of martensite (stroke of ~6.1 mm), which is in the point on the wire surface closest to the spring axis, since tensile and shear stress are maximal there (Fig. 3b). Due to tension/compression asymmetry, first appearance of compression-induced martensite on the opposite side of the surface is retarded to higher stress and also the neutral axis shifts from the center of the cross section of the wire toward the outer surface of the spring. When martensite transformation initiates, distribution of stresses through the wire cross section starts to be quite complex. The tension/compression stress, which is induced by wire bending, combines with shear stress and leads to distinct stress values for initiation of phase transformation at different points on wire cross section. During loading, maxima of shear stress are located on wire surface and follow the shift of the neutral axis. However, positions of maxima of both tensile and compressive stresses move from the surface to the inside, where shear stress component is reduced. During unloading, all stress components reach their maximum values in the inner part of the wire until the full disappearance of martensite (a similar effect during a simple wire unbending was already described in Ref 31) as a consequence of nonlinear hysteretic material behavior and higher strain amplitudes on wire surface, which leads to faster decrease of stress.

4. Experimental

Examined springs were shape set from superelastic 200-μm thin NiTi wires (FWM NiTi#1-SE) using a dedicated fixture and the same heat treatment technology as is usually employed in NiTi stent production (furnace, 510 °C, 10 min) (Ref 32). Figure 2 shows the resulting spring geometry.

For mechanical testing, a self-made device was built up (Fig. 5). The spring was loaded by a linear actuator with maximum speed of 100 mm/s, and force was detected by sensitive 10 N load cell. Thermomechanical coupling and temperature changes can affect significantly the mechanical response of the spring (Ref 33). To ensure isothermal conditions and good heat transfer, samples were measured in water bath with controlled temperature. Although we were not able to detect temperature directly on the wire surface due to a low wire diameter, the isothermal condition was checked indirectly by studying the effect of loading speed on the mechanical response of the spring. It was found that speed effect is negligible even at relatively high loading speeds of 50 mm/s, which was then effectively used in long-term fatigue tests (see Ref 17 for more details). This test also showed acceptable low friction of the seal connecting the sample with the load cell through the wall of the water bath. An in-situ measurement of sample electrical resistivity was also added for automatic detection of possible sample failure. Figures 3 and 4 show resulting force-stroke dependence for spring loading up to two different maximum strokes at temperature 37 °C; Fig. 4 also shows the response at 20 °C for comparison.

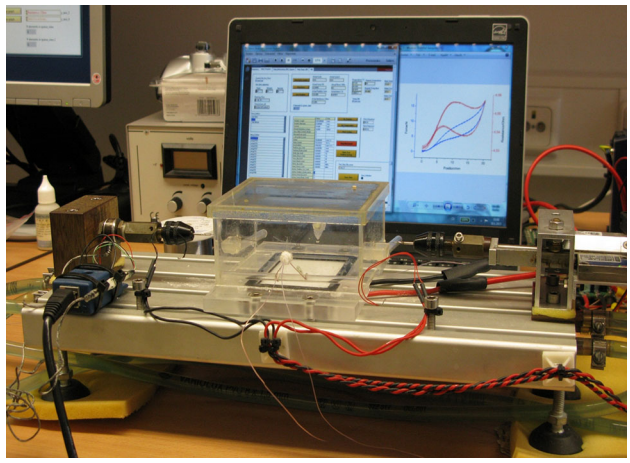

Fig. 5 Experimental setup for mechanical tests of NiTi spring. The spring was placed to water bath to ensure effective temperature control and heat transfer

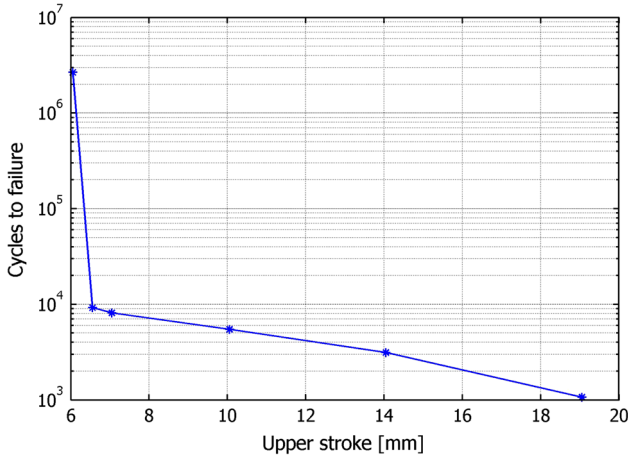

Fig. 6 Dependence of number of cycles to failure of NiTi spring on magnitude of stroke

Fatigue tests were performed at 37 °C in two regimes. In the first one, the spring was cyclically loaded from the stress-free state and the effect of increasing maximum stroke on fatigue resistance was studied. In the second one, the spring was already deformed in the initial state and dependence of fatigue resistance on two parameters—stroke amplitude and initial (=mean) stroke—was investigated. In all cases, tests were repeated three times. Figure 6 shows results of the first test regime; for different maximum strokes, the average number of cycles to failure is plotted. Results of the second regime are plotted as individual points in the plot in Fig. 7. Blue cycle indicates that all samples survived at least 10^5 cycles, and red cross denotes failure of all samples with corresponding numbers of cycles to failure from three independent tests.

5. Discussion

Figures 3 and 4 show a rather good agreement of experimental and simulated responses despite relatively simple

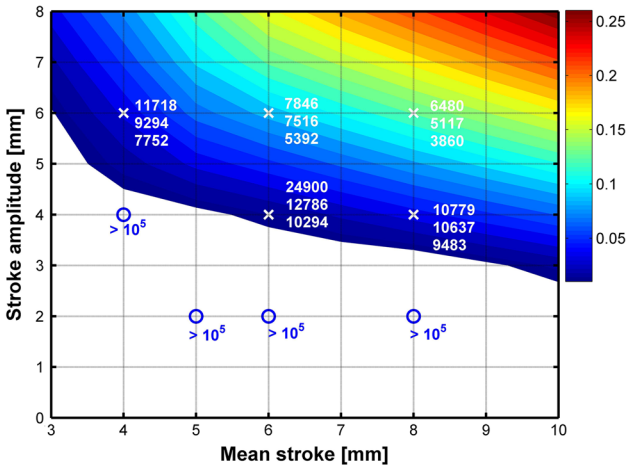

Fig. 7 Number of cycles to failure for different mean strokes and stroke amplitudes (peak to peak). Blue cycles correspond to tests without failure up to 10^5 cycles, crosses with number of cycles to failure to tests in which samples failed during experiment. Color map corresponds to periodic change of volume fraction of martensite according to simulations (Color figure online)

boundary conditions used. Figure 4 also proves effectivity of involving the R-phase to the model. Despite the R-phase transition being described by a simple second-order phase transformation and only entropy and elastic property changes being involved, it can predict temperature dependence of apparent elasticity prior to the conventional martensitic transformation very well.

Figures 4 and 6 provide strong support to the idea that sudden drop in the fatigue resistance is related to the start of martensitic transformation at the most loaded spring part. As loading reaches amplitude in which periodic change of martensite volume fraction is approx. 1%, number of cycles to failure drops by two orders. Subsequent increase of loading amplitude has only a moderate effect and leads to slow decrease of the spring lifetime. This sudden drop of fatigue resistance and sharp boundary between long- and short-life regimes could be probably attributed to inhomogeneous development of martensitic phase transformation and localization of martensite nucleus within austenite/R-phase region, but additional experimental observation and theoretical analysis are needed to verify this explanation.

As shown in Fig. 7, a similar drop of fatigue resistance can be observed even if the spring is cycled around initially deformed state in which a part of the material has already transformed to martensite. The mere existence of initial martensite does not considerably influence the fatigue resistance, but a huge reduction of the lifetime occurs again if the periodic change in martensite volume fraction reaches approx. 1%.

The above conclusions underline the importance of R-phase transformation especially in applications, which work at (almost) constant temperature (e.g., stents in a human body (Ref 34)). If the R-phase transformation precedes martensitic transformation, it considerably decreases effective modulus of material (tangent modulus) between forward and reverse martensitic transformations. This extends the stroke amplitude at which zero periodic change of volume fraction of martensite occurs and thus extends the long-life regime.

6. Conclusions

The main conclusions based on this work can be summarized in the following points:

1. The presented simulations show rather complex stress state distribution, which develops during mechanical loading of a superelastic NiTi spring. This is a consequence of transformation and reorientation processes induced in NiTi by combined tension/compression-shear loading.
2. Simulated results are in a good agreement with experiments, which confirms appropriateness of the utilized model.
3. Comparison of fatigue tests with simulations suggests that the fatigue life depends on the periodic change of martensite fraction during cycling. The lifetime dramatically decreases even when the periodic change in volume fraction of martensite is as small as 1%. Further investigation is needed to elucidate reasons behind this effect.
4. The progress of the mere R-phase transformation (without occurrence of martensitic transformation) does not reduce the fatigue resistance. Moreover, due to significantly lower elasticity of R-phase, its presence in material in cyclic loading can considerably extend range of stroke amplitudes guaranteeing long-life performance of the spring.

Acknowledgments

We would like to thank to prof. T. Ben Zineb for providing access to CLCM computation cluster (Centre Lorrain de calcul haute performance en mécanique, France). This work has been conducted within the institutional project RVO: 61388998 of IT ASCR, v.v.i., and within the CENTEM project CZ.1.05/2.1.00/03.0088. The research has also been supported by the Grant Agency of the Czech Republic through grant projects Nos. 13-13616S, 14-28306P, and 14-15264S and by Academy of Sciences through internal project No. M100761203.

References

1. D.J. Hartl, D.C. Lagoudas, F.T. Calkins, and J.H. Mabe, Use of a Ni60Ti Shape Memory Alloy for Active Jet Engine Chevron Application: I. Thermomechanical Characterization, *Smart Mater. Struct.*, 2009, **19**, p 015020
2. L.G. Machado and M.A. Savi, Medical Applications of Shape Memory Alloys, *Braz. J. Med. Biol. Res.*, 2003, **36**, p 683–691
3. D. Vokoun, D. Majtás, M. Frost, P. Sedlák, and P. Šittner, Shape Memory Hooks Employed in Fasteners, *J. Mater. Eng. Perform.*, 2009, **18**, p 706–710
4. P. Sittner, L. Heller, J. Pilch et al., Roundrobin SMA Modeling, *ESOMAT 2009: The 8th European Symposium on Martensitic Transformations, EDP Sciences*, P. Sittner, L. Heller, and V. Paidar, Eds., 2009, p 08001
5. J. Arghavani, F. Auricchio, R. Naghdabadi, A. Reali, and S. Sohrabpour, A 3-D Phenomenological Constitutive Model for Shape Memory Alloys Under Multiaxial Loadings, *Int. J. Plast.*, 2010, **26**, p 976–991
6. Y. Chemisky, A. Duval, E. Patoor, and T. Ben Zineb, Constitutive Model for Shape Memory Alloys Including Phase Transformation, Martensitic Reorientation and Twins Accommodation, *Mech. Mater.*, 2011, **43**, p 361–376

7. D.C. Lagoudas, D.J. Hartl, Y. Chemisky, L.G. Machado, and P. Popov, Constitutive Model for the Numerical Analysis of Phase Transformation in Polycrystalline Shape Memory Alloys, *Int. J. Plast.*, 2012, **32–33**, p 155–183
8. M. Panico and L.C. Brinson, A Three-Dimensional Phenomenological Model for Martensite Reorientation in Shape Memory Alloys, *J. Mech. Phys. Solids*, 2007, **55**, p 2491–2511
9. Z. Moumni, W. Zaki, and Q.S. Nguyen, Theoretical and Numerical Modeling of Solid-Solid Phase Change: Application to the Description of the Thermomechanical Behavior of Shape Memory Alloys, *Int. J. Plast.*, 2008, **24**, p 614–645
10. A.F. Saleeb, S.A. Padula, and A.A. Kumar, A Multi-Axial, Multi-mechanism Based Constitutive Model for the Comprehensive Representation of the Evolutionary Response of SMAs Under General Thermomechanical Loading Conditions, *Int. J. Plast.*, 2011, **27**, p 655–687
11. L. Saint-Sulpice, S. Arbab Chirani, and S. Calloch, A 3D Super-Elastic Model for Shape Memory Alloys Taking into Account Progressive Strain Under Cyclic Loadings, *Mech. Mater.*, 2009, **41**, p 12–26
12. P. Sedlak, M. Frost, B. Benesova, P. Sittner, and T. Ben Zineb, Thermomechanical Model for NiTi-Based Shape Memory Alloys Including R-phase and Material Anisotropy Under Multi-Axial Loadings, *Int. J. Plast.*, 2012, **39**, p 132–151
13. C. Liang, A Rogers Design of Shape Memory Alloy Actuators, *J. Intell. Mater. Syst. Struct.*, 1997, **8**, p 303–313
14. Y. Toi, J.-B. Lee, and M. Taya, Finite Element Analysis of Superelastic, Large Deformation Behavior of Shape Memory Alloy Helical Springs, *Comput. Struct.*, 2004, **82**, p 1685–1693
15. R. Mirzaeifar, R. DesRoches, and A. Yavari, A Combined Analytical, Numerical, and Experimental Study of Shape-Memory-Alloy Helical Springs, *Int. J. Solids Struct.*, 2011, **48**, p 611–624
16. A.F. Saleeb, B. Dhakal, M.S. Hosseini, and S.A. Padula, Large Scale Simulation of NiTi Helical Spring Actuators Under Repeated Thermomechanical Cycles, *Smart Mater. Struct.*, 2013, **22**, p 094006
17. K. Hirmanova, J. Pilch, J. Racek, L. Heller, P. Sittner, L. Recman, M. Petrenec, and P. Sedlak, Physical Simulation of the Random Failure of Implanted Braided NiTi Stents, *J. Mater. Eng. Perform,* accepted in
18. A. Sadjadpour and K. Bhattacharya, A Micromechanics-Inspired Constitutive Model for Shape-Memory Alloys: the One-Dimensional Case, *Smart Mater. Struct.*, 2007, **16**, p S51–S62
19. C. Grabe and O.T. Bruhns, On the Viscous and Strain Rate Dependent Behavior of Polycrystalline NiTi, *Int. J. Solids Struct.*, 2008, **45**, p 1876–1895
20. Q.S. Nguyen, *Stability and Nonlinear Solid Mechanics*, John Wiley, New York, 2000, p 17–40
21. K. Hackl and F.D. Fischer, On the Relation Between the Principle of Maximum Dissipation and Inelastic Evolution Given by Dissipation Potentials, *Proc. R. Soc. A*, 2008, **464**, p 117–132
22. M. Frost, B. Benesova, and P. Sedlak, A Microscopically Motivated Constitutive Model for Shape Memory Alloys: Formulation, Analysis and Computations, *Math. Mech. Solids*, accepted in
23. S. Qiu, B. Clausen, S.A. Padula, R.D. Noebe, and R. Vaidyanathan, On Elastic Moduli and Elastic Anisotropy in Polycrystalline Martensitic NiTi, *Acta Mater.*, 2011, **59**, p 5055–5066
24. P. Sittner, M. Landa, P. Lukas, and V. Novak, R-phase Transformation Phenomena in Thermomechanically Loaded NiTi Polycrystals, *Mech. Mater.*, 2006, **38**, p 475–492
25. K. Gall, H. Sehitoglu, Y.I. Chumlyakov, and I.V. Kireeva, Tension-Compression Asymmetry of the Stress-Strain Response in Aged Single Crystal and Polycrystalline NiTi, *Acta Mater.*, 1999, **43**, p 1203–1217
26. V. Grolleau, H. Louche, V. Delobelle, A. Penin, G. Rio, Y. Liu, and D. Favier, Assessment of Tension-Compression Asymmetry of NiTi Using Circular Bulge Testing of Thin Plates, *Scr. Mater.*, 2011, **65**, p 347–350
27. S.C. Mao, J.F. Luo, Z. Zhang, M.H. Wub, Y. Liu, and X.D. Han, EBSD Studies of the Stress-Induced B2-B19' Martensitic Transformation in NiTi Tubes Under Uniaxial Tension and Compression, *Acta Mater.*, 2010, **58**, p 3357–3366
28. Y.C. Shu and K. Bhattacharya, The Influence of Texture on the Shape-Memory Effect in Polycrystals, *Acta Mater.*, 1998, **46**, p 5457–5473
29. B. Reedlunn, C.B. Churchill, E.E. Nelson, J.A. Shaw, and S.H. Daly, Tension, Compression, and Bending of Superelastic Shape Memory Alloy Tubes, *J. Mech. Phys. Solids*, 2014, **63**, p 506–537
30. S. Miyazaki and K. Otsuka, Deformation and Transition Behavior Associated with the R-phase in Ti-Ni Alloys, *Metall. Trans. A*, 1986, **17A**, p 53–63
31. T. Atanacković and M. Achenbach, Moment-Curvature Relations for a Pseudoelastic Beam, *Contin. Mech. Thermodyn.*, 1989, **1**(1), p 73–80
32. Ella-CS s.r.o., http://www.ellacs.eu/stents.html
33. R. Mirzaeifar, R. DesRoches, A. Yavari, and K. Gall, Coupled Thermo-Mechanical Analysis of Shape Memory Alloy Circular Bars in Pure Torsion, *Int. J. Non-Linear Mech.*, 2012, **47**, p 118–128
34. M. Frost, P. Sedlak, A. Kruisova, and M. Landa, Simulations of Self-Expanding Braided Stent Using Macroscopic Model of NiTi Shape Memory Alloys Covering R-Phase, *J. Mater. Eng. Perform.*, submitted to